

A Waveguide Orthomode Transducer for 385-500 GHz

A. Navarrini¹, C. Groppi², and G. Chattopadhyay³

¹*INAF-Cagliari Astronomy Observatory, Italy*

²*ASU School of Earth and Space Exploration, USA*

³*NASA-Jet Propulsion Laboratory, USA*

* Contact: navarrin@ca.astro.it, phone +39-070-711 80 218

Abstract— We describe the design, construction, and performance of a waveguide Orthomode Transducer (OMT) for the 385-500 GHz band. The OMT is based on a symmetric backward coupling structure and has a square waveguide input (0.56x0.56 mm²) and two single-mode waveguide outputs: a standard WR2.2 waveguide (0.56x0.28 mm²) and an oval waveguide with full-radius corners. The OMT is rescaled from a lower frequency design that was developed for the 3 mm band; it was optimized using a commercial 3D electromagnetic simulator.

The OMT consists of two mechanical blocks in split-block configuration that were fabricated using conventional CNC milling machine. A first prototype copper alloy OMT employing standard UG387 flanges at all ports was fabricated and tested. From 385 to 500 GHz the measured input reflection coefficient was less than -10 dB, the isolation between the outputs was less than -25 dB, the cross polarization was less than -10 dB, and the transmission was \approx 2 dB at room temperature for both polarization channels.

The effects of misalignment errors in the OMT performance were studied using electromagnetic simulation.

A second OMT version utilizing custom made mini-flanges and much shorter waveguides was designed and will be tested soon. This novel OMT is more tolerant to misalignment errors of the block halves and is expected to have much improved performance over the first prototype.

I. INTRODUCTION

An Orthomode Transducer (OMT) is a passive device that separates two orthogonal linearly polarized signals within the same frequency band. An OMT has three physical ports but exhibits properties of a four-port device because the input common port, usually a waveguide with a square or circular cross-section, provides two electrical ports that correspond to the independent orthogonal polarized signals. In modern radio-astronomy receivers, requirements of the OMT are a high cross-polarization discrimination between the orthogonal signals, low insertion loss, and a good match of all electrical ports over relative bandwidths of 30% or wider. Several asymmetric OMTs have been designed to cover

bandwidths of less than 30% [1]-[2]. Highly symmetric structures are required to avoid the excitation of higher order modes and achieve broad bandwidth (up to 40% or wider.)

Because the small dimensions and tight tolerances pose a significant challenge for the fabrication and assembly of the parts, only few broadband OMT designs have been demonstrated to work well at frequencies greater than \approx 100 GHz. These designs are based on: *a*) the two-fold symmetric Bøifot junction [3]-[6] adopted for ALMA Band 3 (84-116 GHz) and Band 6 (211-275 GHz); *b*) the four-fold symmetric turnstile junction [7]-[9] adopted for CARMA 200-270 GHz and Clover 75-110 GHz; *c*) the double ridged Bøifot-type junction [10]-[11] adopted for ATNF 70-117 GHz and for ALMA Band 4 (125-163 GHz), Band 5 (163-211 GHz), and Band 8 (385-500 GHz); *d*) the reverse-coupling waveguide junction [12]-[13] adopted for the 84-116 GHz band of the Sardinia Radio Telescope.

In particular, the highest frequency range for which a broadband OMT has been developed and employed in a large project is the 385-500 GHz of ALMA Band 8 [14]; the OMT is based on a double ridged Bøifot-type junction.

Alternative OMT designs based on finline [15] or planar structures have also been proposed for use at millimetre and submillimetre wavelengths.

Here, we present the design and performance of two waveguide OMT prototypes for the 385-500 GHz band which are based on a symmetric reverse-coupling architecture. The first OMT prototype, presented in Sec. II, utilizes standard UG387 flanges and has long input and output waveguide sections. The second OMT prototype, presented in Sec. III, utilizes custom made mini-flanges, has much shorter input and output waveguides, and is more tolerant to misalignment errors of the mechanical blocks.

II. FIRST OMT PROTOTYPE

A. Architecture of the first OMT prototype

The design of our first 385-500 GHz OMT is directly rescaled from the lower frequency device developed for the 3 mm band (84-116 GHz band) presented in [13]. Our 385-500 GHz waveguide OMT, illustrated in Fig. 1, is based

on a reverse-coupling structure and consists essentially of: *a*) a 0.56x0.56 mm² square waveguide input (Port 1) that transitions to a full-height WR2.2 (0.56x0.28 mm²) rectangular waveguide through a two-section transformer; the transformer is followed by a 90 deg E-plane rectangular-to-oval waveguide bend; *b*) two symmetric 90^o waveguide hybrid couplers on the sidearms utilizing reactively terminated ports (dual-side backward coupler); *c*) an E-plane 180^o waveguide hybrid (Y-junction) to recombine the out-of-phase signals from the two backward coupling structures.

The OMT single-mode waveguide outputs are: *a*) an oval waveguide with full-radius corners and external cross-section 0.62x0.28 mm² for Pol 1 (Port 2); *b*) a standard WR2.2 rectangular waveguide for Pol 2 (Port 3.)

The square waveguide input propagates two orthogonal linear polarized signals Pol 1 and Pol 2 associated, respectively, with the TE₁₀ and TE₀₁ fundamental modes, when the wavelength is below the cut-off value $\lambda_c(TE_{10})=2a=1.12$ mm (frequencies above $\nu_c=267.67$ GHz.) Besides the fundamental modes, higher order modes can propagate in the square waveguide in the 385-500 GHz frequency band of interest. These are the TE₁₁ and TM₁₁ that have the same cut-off frequency of $\nu_c=378.55$ GHz. In theory, these modes can be excited by the discontinuity created by the apertures (slots) of the sidearms. However, their excitation can be avoided as long as the two-fold symmetry of the structure is maintained. The adopted symmetry enables broadband operation allowing to achieve a relative bandwidth for the device larger than ~30 %.

The symmetric coupling structure in the common square waveguide arm splits, with opposite phases, the incoming Pol 2 signal in the two rectangular waveguide sidearms. Signal coupling to each sidearm is obtained with a broadband 90^o hybrid coupler realized as a 3-dB E-plane branch-line coupling structure with four branches. The four 0.10 mm wide apertures through the broad walls of the waveguide sidearms are equally spaced of 0.072 mm (see details in Fig. 2.) The branches have a length of 0.178 mm. The through port and the coupled port of each hybrid are terminated with reactive loads for Pol 2. In the common arm, the reactive load is provided by a two-section transformer polarization discriminator that reflects back all Pol 2 power in the 385-500 GHz frequency range of design. Indeed, the output rectangular waveguide section of such transformer has size 0.56x0.28 mm² that cuts off the propagation of the TE₀₁ mode associated with Pol 2 to frequencies above $\nu_c(TE_{01})=535.34$ GHz, outside our operating range. On the other hand, the orthogonal polarization, Pol 1, is relatively unaffected by the presence of both the branch-line apertures in the two sidearms and of the common arm two-section transformer. Each section of such transformer is approximately a quarter wavelength long. Therefore, Pol 1 is well matched to the output and is fully coupled (forward coupling) to an E-plane 90 deg bend transition that brings out, orthogonal to the main arm, the oval cross section port; the oval waveguide is easy to machine with an end-mill and can be attached to a standard WR2.2 waveguide producing a

negligible power reflection (return loss >38 dB across 385-500 GHz.)

The two Pol 2 signals emerging backward with -3 dB power from the sidearms of the reverse-coupling structure travel through two symmetric waveguide paths. Each Pol 2 signal travels through a 180 deg WR2.2 waveguide E-plane bend (0.96 mm inner diameter), a straight waveguide section (length of 2.2 mm), and a 90 deg waveguide E-plane bend (0.85 mm inner diameter;) the two Pol 2 signals are recombined by an E-plane Y-junction power combiner with standard WR2.2 output whose axis is coincident with the one

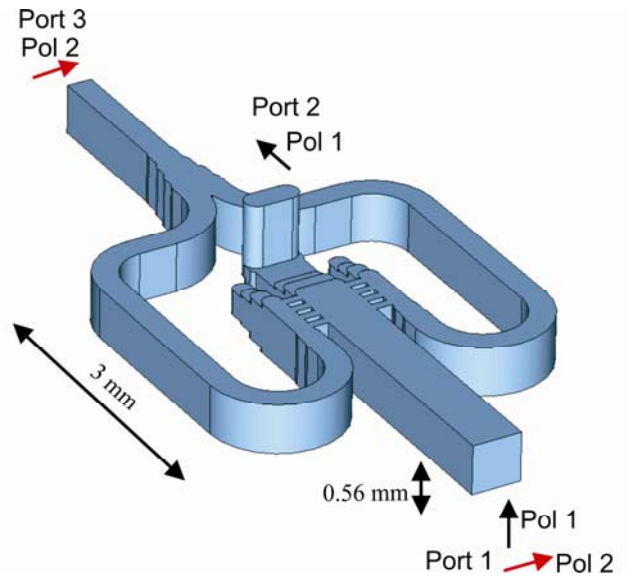


Fig. 1. Internal view of the symmetric dual-side backward coupler OMT.

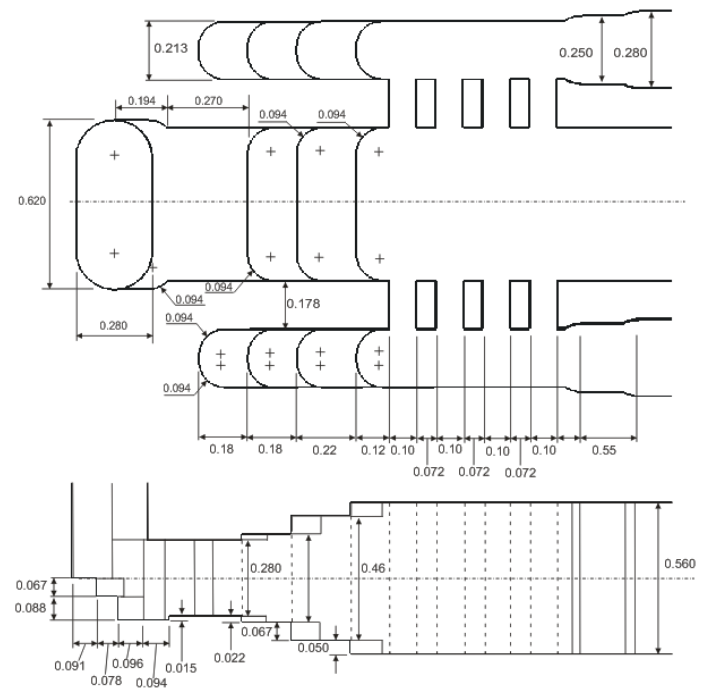


Fig. 2. Cutout views with dimensions (in mm) of the symmetric backward couplers of Fig. 1. The structure was optimized for operation in the 385-500 GHz band.

of the square waveguide input. The combiner is based on a design by Kerr [16].

In the rectangular waveguide sidearms, the reactive loads for Pol 2 are provided by a short circuited three-step H-plane discontinuity (two transformer sections.) The transformer sections have the same physical length and height in the sidearms and in the common arm to guarantee that Pol 2 sees the same impedance when looking toward the through and coupled ports of the hybrids. This allows the split Pol 2 signals, which are reflected backward by the reactive loads, to recombine out-of-phase in the common arm (thus providing a destructive interference with low reflection at the common port) and in-phase in the two opposite sidearms. The constructive interference of the backward waves provides a coupling of -3 dB to each rectangular output port. Pol 2 signals at these two ports are 180° out-of-phase to each other because the E-field signal at the common square input couples to the two sidearm hybrids in opposite directions. The rectangular waveguide sidearms have a reduced height in the coupling section of the hybrids (0.213 mm rather than full 0.280 mm) in order to increase the bandwidth of the device.

The waveguide steps of the two-section transformers have round corners (radius 0.094 mm) to allow easy machining of the parts with an end-mill. Each reduced-height rectangular waveguide sidearm carrying the reverse-coupled -3 dB Pol 2 signal is transformed to a standard WR2.2 full-height 0.56×0.28 mm² waveguide at the hybrid signal output. This is accomplished by a single-section quarter-wave transformer, 0.55 mm long.

The electrical performance of the OMT was optimized using the commercial electromagnetic simulator CST Microwave Studio¹ based on the finite integration technique.

B. Electromagnetic simulation of the first OMT prototype

The first OMT prototype has long input and output waveguides (see Fig. 3) with lengths, respectively 11.3 mm and 10.8 mm. This OMT utilizes standard UG387 flanges. The physical length of the waveguide circuit of the OMT from input to output ports is approximately 14 mm for Pol 1 and 31 mm for Pol 2.

The simulation results for the reflected amplitude of the two independent fundamental modes TE₁₀ (Pol 1) and TE₀₁ (Pol 2) at the square waveguide input of the device of Fig. 3 are illustrated in Fig. 4. The reflection coefficient is below -17 dB for both polarizations over the entire band of interest.

The simulated transmission losses at 300 K and at 4 K of the two polarization channels of the OMT are shown in Fig. 5. In the simulation, we assumed the waveguide conductor to have perfectly smoothed walls with conductivities $\sigma=4.26 \cdot 10^7 \Omega^{-1}m^{-1}$ at 300 K (same as the dc conductivity of Gold) and $\sigma=10.0 \cdot 10^7 \Omega^{-1}m^{-1}$ at 4 K. The simulated transmissions are about -0.35 dB for Pol 1 and about -1 dB

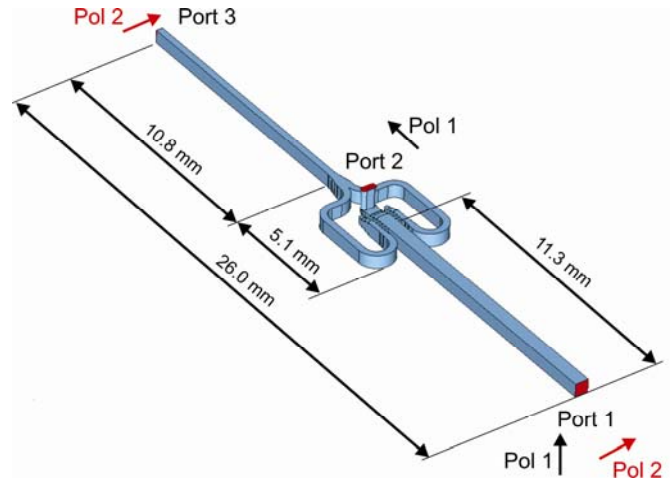


Fig. 3. Full view of the inner parts of the first OMT prototype showing the long square waveguide input (11.3 mm) and rectangular waveguide output (10.8 mm) of the reverse-coupling structure. The oval waveguide has a length of only 1 mm.

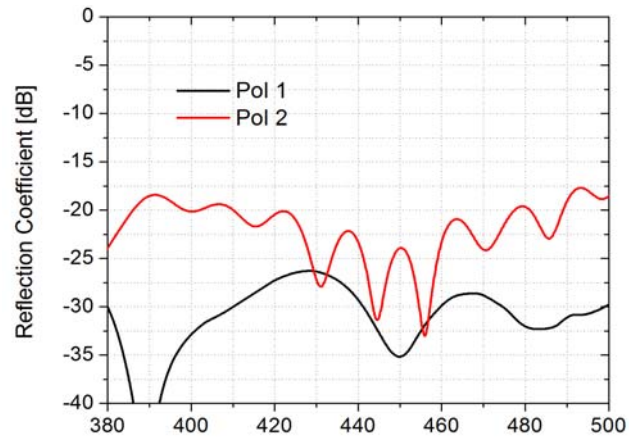


Fig. 4. Simulated reflection coefficient at the common waveguide port of the three-port device illustrated in Fig. 3.

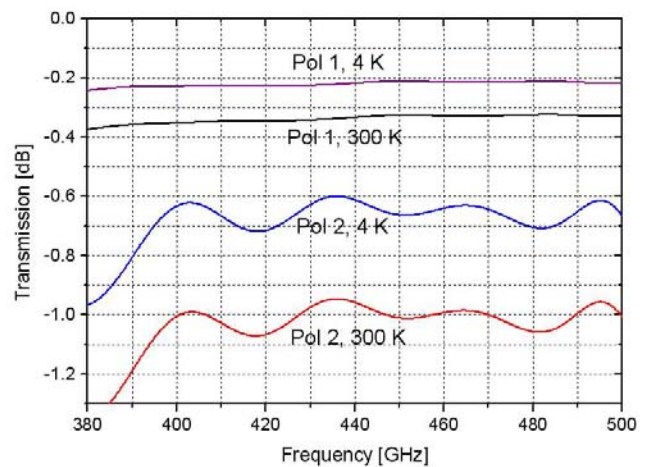


Fig. 5. Simulated transmissions of the full OMT illustrated in Fig. 3.

¹ CST Microwave Studio, Darmstadt, Germany.

for Pol 2 at 300 K. Under these assumptions the losses at 4 K reduce to $(4.26/10)^{0.5} \approx 64\%$ of the 300 K values.

To evaluate the contribution to the OMT insertion loss due to the input and output waveguide sections of the device, we simulated the loss of a straight section of a 11.3 mm long $0.56 \times 0.56 \text{ mm}^2$ square waveguide and of a 10.8 mm long WR2.2 waveguide. The simulation results across 385-500 GHz, shown in Fig. 6, indicate that the losses at 300 K are $\approx 0.2 \text{ dB/cm}$ and $\approx 0.3 \text{ dB/cm}$ for, respectively the square waveguide and the WR2.2 waveguide. Therefore, in the OMT, more than half of the room temperature insertion loss of Pol 1 is due to the square waveguide input, and about half of the insertion loss of Pol 2 is due to the square waveguide input plus rectangular waveguide output.

The cross-polarization and isolation levels of the OMT is expected to be zero ($-\infty \text{ dB}$) for the perfectly symmetric model of Fig. 3. The extremely low but finite value (less than -100 dB) obtained from simulation is due to the numerical rounding off errors in the computation.

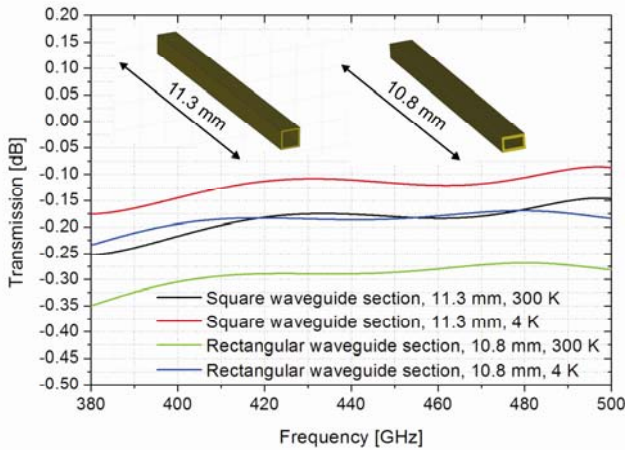


Fig. 6. Simulated transmissions loss of 11.3 mm long square waveguide (cross-section $0.56 \times 0.56 \text{ mm}^2$) and 10.8 mm long WR2.2 rectangular waveguide (cross-section $0.56 \times 0.28 \text{ mm}^2$) at 300 K and 4 K.

C. Mechanical blocks of the first OMT prototype

The OMT consists of two mechanical blocks and is fabricated by splitting the structure of Fig. 3 along the E-plane of the side-coupled rectangular waveguides. The device has external dimensions $19 \times 26 \times 28 \text{ mm}^3$ and accepts standard UG387 flanges at all ports. A circular pocket (diameter 20 mm, depth 8.5 mm) is machined into one of the blocks to reduce the oval waveguide to a length of only 1 mm. Photographs of the assembled OMT and of the two unassembled OMT blocks are shown, respectively in Fig. 7 and Fig. 8. The blocks were fabricated in 145 Copper alloy (unplated) using a Kern Micro numerically controlled milling machine at University of Arizona.

Photographs of the internal details of the blocks are shown in Figs. 9-10. The blocks were aligned using two precision $1/16''$ diameter dowel pins. The tolerances for the waveguide channels in the two blocks and of the alignment between the blocks were specified at $\pm 5 \mu\text{m}$. The blocks are bolted together by four 4-40 stainless steel screws.

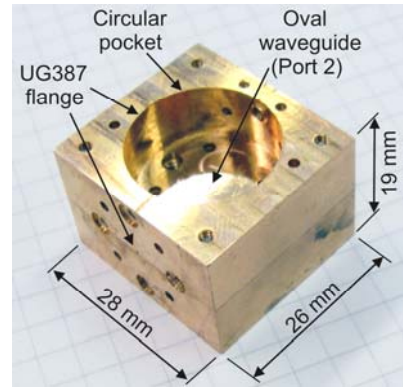


Fig. 7. Photograph of the assembled OMT (first prototype) with UG387 flanges at all ports.

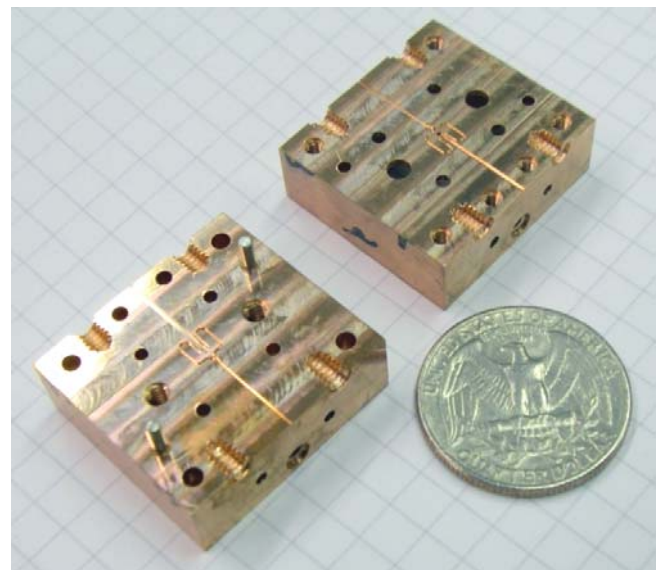


Fig. 8. Photograph of the two unassembled blocks of the first OMT prototype showing the internal waveguide circuitry.

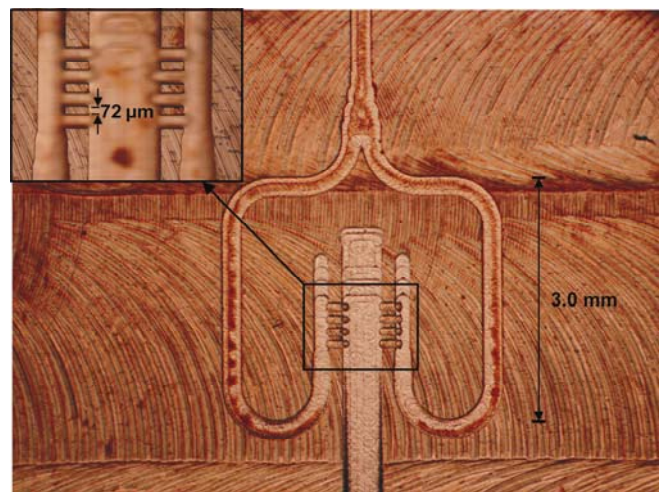


Fig. 9. Photograph of the internal details of one of the OMT blocks showing the dual-backward coupler waveguide circuitry and the three metal "teeth" between branch-line slots on both sidearms (close-up view.) The oval waveguide is also visible on the right.



Fig. 10. Detail of the three metal “teeth” between branchline slots of one of the coupler sidearms.

D. Experimental results of the first OMT prototype

The OMT was tested at JPL (Jet Propulsion Laboratory) using a Vector Network Analyser (VNA) consisting of a HP8510C Network Analyser and submillimeter-wave OML test set extensions. The VNA was calibrated at the WR2.2 rectangular waveguides outputs of the extension heads using two-port calibrations with WR2.2 calibration kit. The calibration procedure was used to remove systematic instrumental effects and to calibrate out the response of the instrument up to the chosen calibration planes (see Fig. 11.) Additional measurement of two pairs of identical back-to-back WR2.2 waveguide-to-square waveguide transition² (3/4” long, linearly tapered from one end to the other, with UG387 flanges at both sides) allowed to calibrate out their individual effects and to derive the S-parameters of the OMT at the physical ports of the device.

A schematic of the Pol 2 transmission test setup is shown in Fig. 11. The square waveguide input of the OMT was attached to the WR2.2 waveguide port of the network analyser (Port 1) through the WR2.2 waveguide-to-square waveguide transition. The transition was oriented to excite the Pol 2 in the OMT. The WR2.2 waveguide output of the OMT was attached to the second WR2.2 waveguide port of the analyser (Port 2.) The oval waveguide of the OMT was terminated with a matched WR2.2 waveguide. The transmission measurement of the other polarization channel was obtained with a setup similar to the one in Fig 11 but with WR2.2 waveguide-to-square waveguide transition rotated by 90 deg to excite Pol 1 at the OMT input and with waveguide matched load and second port of the analyser swapped at the OMT outputs. A photograph of the transmission test setup of Pol 1 is shown on Fig. 12.

The measured transmissions of the OMT are illustrated in Fig. 13. The average measured transmission of the OMT is ≈ -1.7 dB for Pol 1 and ≈ -2.2 dB for Pol 2, much larger in overall level of the values predicted by simulation (see Fig. 5.)

The reflection coefficient at the OMT input port was measured for both polarizations by terminating the OMT outputs with WR2.2 matched loads. The amplitude of the measured reflection is below -10 dB for both polarization channels (Fig. 14.)

An estimate of the isolation was obtained by measuring the transmissions from the OMT output ports with its square waveguide input port open to free space. This gives an upper

limit of the isolation of the device. The measured isolation is below -25 dB (Fig. 15.)

The cross-polarization of the OMT is the transmission from one polarization channel at the square waveguide input to the unwanted output channel when the other two electrical ports (of the four electrical ports device) are terminated into a matched load. We estimated the cross-polarization of the OMT by using a transmission setup similar to the one in Fig. 12, where the square waveguide-to-rectangular waveguide transition is connected to VNA port 1 to inject one polarization signal at the OMT square waveguide input port, the VNA port 2 is connected to the “unwanted” OMT output, and the second OMT output is terminated into a WR2.2 matched load. The measured cross polarization level is below -10 dB across the band of interest (Fig. 16.)

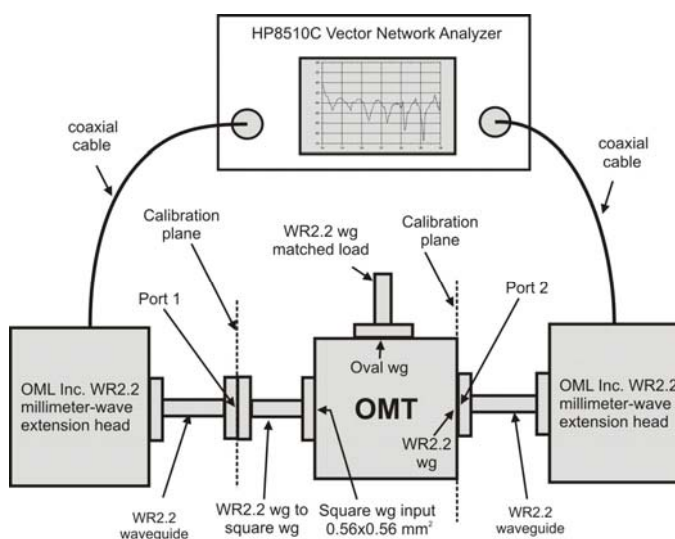


Fig. 11. S-parameter measurement of the OMT with the vector network analyser. The particular configuration refers to the transmission measurement of Pol 2.



Fig. 12. Photo of the OMT during Pol 1 transmission measurement with the vector network analyser.

² Radiometer Physics GmbH, Germany.

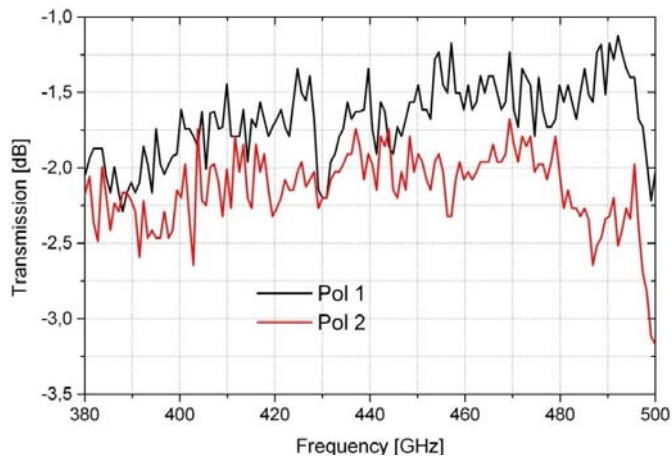


Fig. 13. Measured transmissions of the first OMT prototype (at room temperature.)

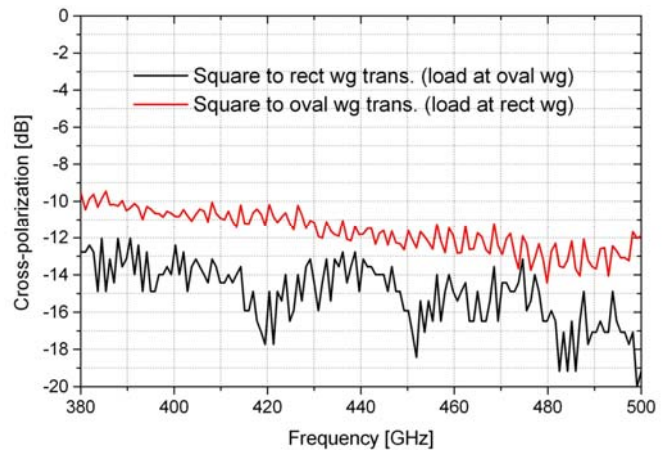


Fig. 16. Measured cross-polarization of the first OMT prototype.

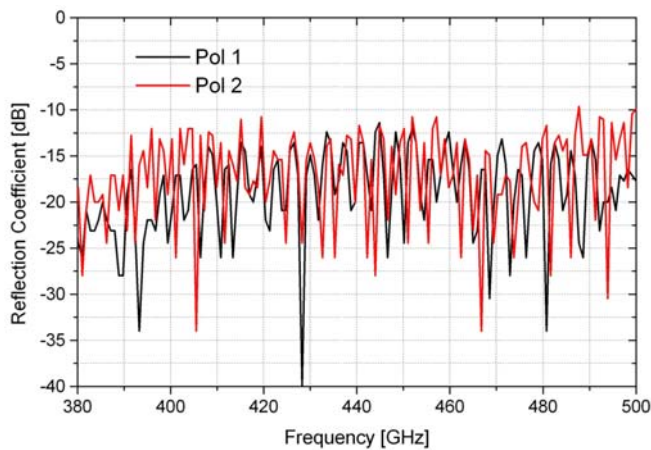


Fig. 14. Measured input reflections of OMT (first prototype.)

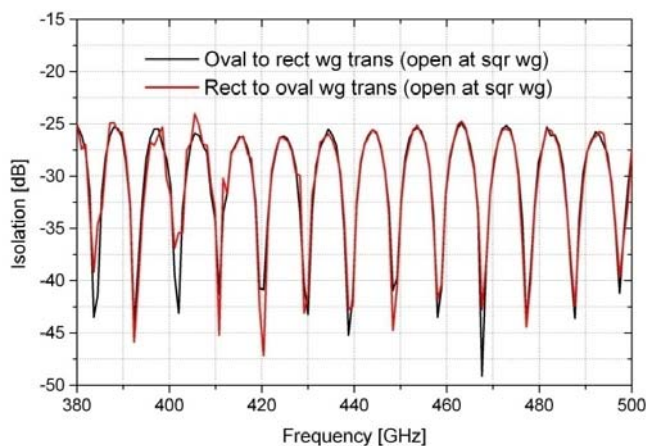


Fig. 15. Measured upper limit of the isolation of the OMT (first prototype): transmission between output ports with square waveguide input open to free space.

E. Electromagnetic simulation of misaligned square waveguides

The measured performance of the first OMT prototype are clearly inferior to what expected from the electromagnetic simulation of the “ideal” device of Fig. 3. As a first step to understand the observed differences between simulation and measure, we estimated, using simulation, the contribution to the cross-polarization due to a lateral misalignment δ of a square waveguide section of length l (see Fig. 17) as it would result from a lateral shift of two block halves. The cross-polarization is, in this case, the coupling between Pol 1 at one end and Pol 2 at the other end of the square waveguide.

The cross-polarization was simulated for misaligned square waveguides with cross-section $0.56 \times 0.56 \text{ mm}^2$ (guided wavelength $\lambda_g \approx 0.86 \text{ mm}$ around the central frequency of 440 GHz.) We used waveguide lengths $l=11.3 \text{ mm}$ (same as the input waveguide section of the OMT, $\approx 13 \lambda_g$), $l=2 \text{ mm}$ ($\approx 2.3 \lambda_g$), and lateral misalignments δ of 2 and 5 μm .

The simulation results are shown in Fig. 18. We can see that for $l=11.3 \text{ mm}$, even a misalignment as small as $\delta=5 \mu\text{m}$ generates a cross-polarization level of $\approx -10 \text{ dB}$, which is of the same level of the one measured in the OMT. Reducing the square waveguide length down to $l=2 \text{ mm}$ decreases the cross-polarization level to $\approx -25 \text{ dB}$ (using the same $\delta=5 \mu\text{m}$.) If we could reduce the misalignment to $\delta=2 \mu\text{m}$ in a waveguide with $l=2 \text{ mm}$ the cross-polarization would decrease to $\approx -33 \text{ dB}$.

Therefore, for a given misalignment δ , the cross-polarization level is greater for a longer waveguide, while for a given waveguide length l , the cross-polarization level is greater for a larger misalignment.

In conclusion, the cross-polarization level can be minimized by choosing the shortest possible square waveguide length at the OMT input.

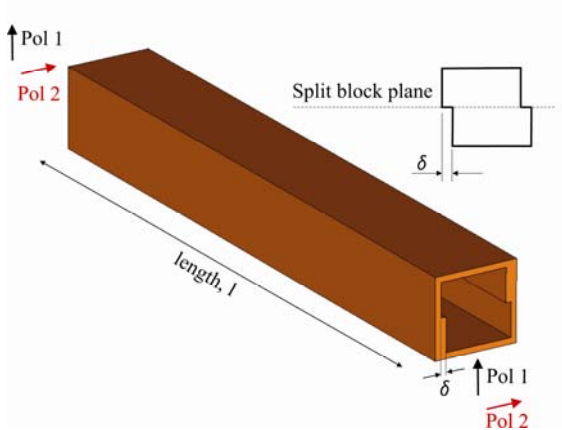


Fig. 17. Square waveguide of length l with lateral misalignment δ along the E-plane of Pol 2.

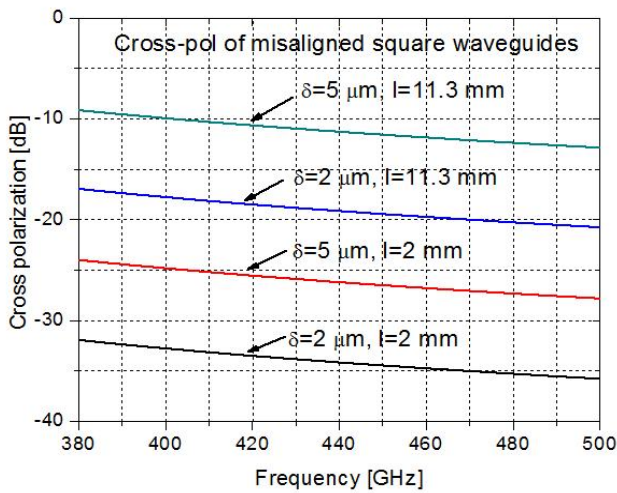


Fig. 18. Simulated cross-polarization of $0.56 \times 0.56 \text{ mm}^2$ square waveguides, $l=11.3 \text{ mm}$ and $l=2 \text{ mm}$ long, with lateral misalignments δ of $2 \text{ }\mu\text{m}$ and $5 \text{ }\mu\text{m}$.

F. Electromagnetic simulation of misaligned OMT (first prototype)

We performed electromagnetic simulation of a full structure of the first OMT prototype, as in Fig. 3, where the two OMT block halves are laterally misaligned of $\delta=2 \text{ }\mu\text{m}$ and $5 \text{ }\mu\text{m}$.

The simulation result for the transmissions of the two polarization channels with OMT blocks misaligned by $5 \text{ }\mu\text{m}$ is shown in Fig. 19. The transmissions, of order -1 dB and -1.7 dB for, respectively Pol 1 and Pol 2, are considerably worse than those expected from the perfectly aligned device (see Fig. 5), and are quite close to the measured values (see Fig. 13.)

The simulated input reflection of the OMT, misaligned by $5 \text{ }\mu\text{m}$, is shown in Fig. 20. As we can see, except for a relatively small increase in reflection of Pol 1, the overall levels remain below -20 dB across most of the band, similar to the simulated value of the perfectly aligned device (see Fig. 4.)

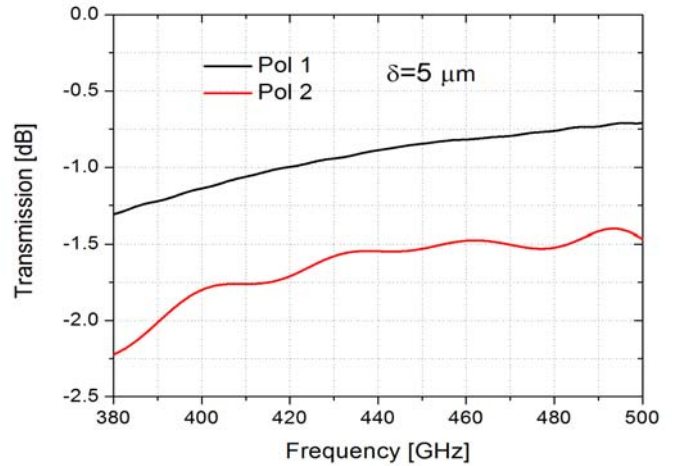


Fig. 19. Simulated transmissions of the first OMT prototype of Fig. 3 with lateral misalignments $\delta=5 \text{ }\mu\text{m}$. We assumed the waveguide conductor to have perfectly smoothed walls with conductivities $\sigma=4.26 \cdot 10^7 \text{ }\Omega^{-1}\text{m}^{-1}$ (300 K.)

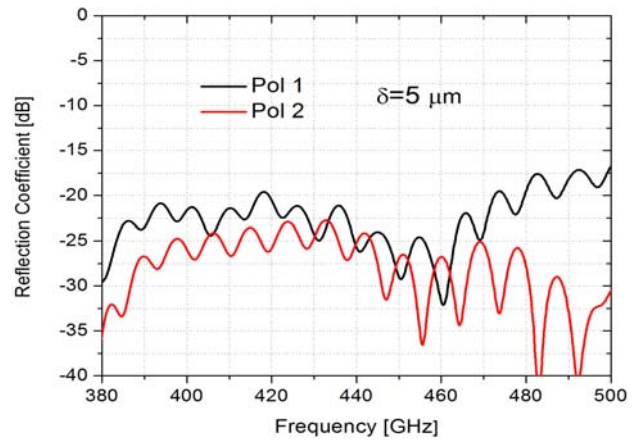


Fig. 20. Simulated input reflection coefficient of the first OMT prototype of Fig. 3 with lateral misalignments $\delta=5 \text{ }\mu\text{m}$.

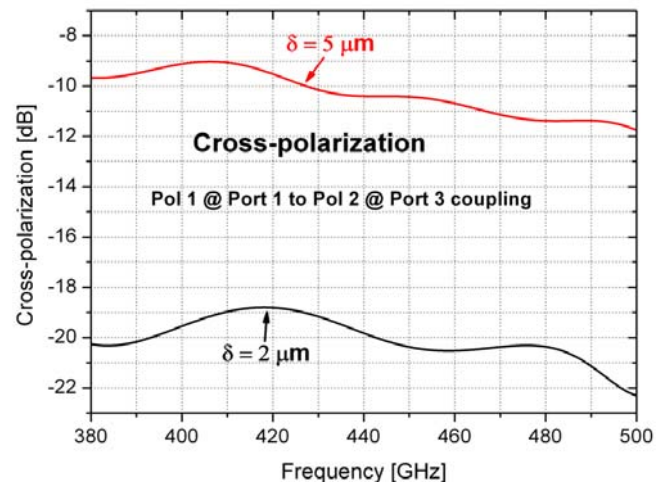


Fig. 21. Simulated cross-polarization of the full OMT of Fig. 7 with lateral misalignments δ of $2 \text{ }\mu\text{m}$ and $5 \text{ }\mu\text{m}$.

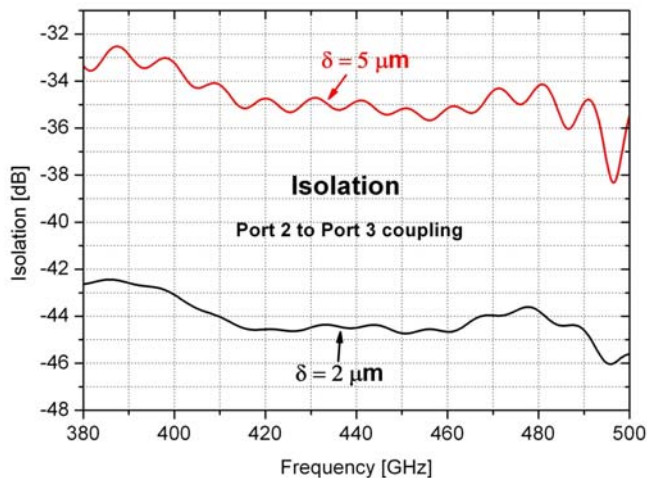


Fig. 22. Simulated isolation of the full OMT of Fig. 7 with lateral misalignment δ of 2 μm and 5 μm .

The results of the electromagnetic simulation for the cross-polarization and isolation of the OMT misaligned of $\delta=2$ and 5 μm are shown, respectively in Fig. 21 and Fig. 22. With a misalignment of $\delta=5 \mu\text{m}$, the cross-polarization is approximately -10 dB, similar in overall level to the measured value as well as to the value resulting from the simulation of a 11.3 mm long square waveguide laterally misaligned by the same δ . This implies that, in a laterally misaligned OMT, most of the cross-polarization is due to the misalignment of the common square waveguide of the device rather than to the misalignment of the remaining parts (i.e. of the reverse-coupling structure.)

The simulated isolation is of the order of -35 dB when $\delta=5 \mu\text{m}$. Both cross-polarization and isolation decrease, respectively to ≈ -20 dB and ≈ -44 dB if $\delta=2 \mu\text{m}$.

In addition to the effects of misaligned block halves of the OMT, the cross-polarization level also depends on the misalignment of square waveguide joints [17] between OMT input and its connecting element (for example a square waveguide-to-rectangular waveguide transition used for test or a feed-horn used in a radioastronomy receiver.) The measured cross-polarization value of the OMT is due to the combined effects of the various misalignments as well as of the internal mechanical imperfections and small asymmetries in the OMT structure.

III. SECOND OMT PROTOTYPE

The simulation results presented in Sec. II E and F indicate that the OMT performance can be considerably improved by decreasing the length of the square waveguide input section of the device. Therefore, we decided to design a second OMT prototype with an input waveguide length l as short as possible. We adopted custom made mini-flanges at all ports and were able to reduce l to 2 mm. In the new design, shown in Fig. 23, the oval waveguide output was moved further away from the input. A shorter output waveguide (4.8 mm long) was also used. The physical length of the waveguide circuit of the new OMT from input to output ports is approximately 6.5 mm for Pol 1 and 20 mm for Pol 2,

respectively 46% and 65% of the lengths used in the first OMT prototype.

The alignment pins and screw holes of the mini-flange are on a 7.11 mm (0.28") bolt circle. A slightly modified Y-junction 180° power combiner and additional waveguide bends in the sidearms are used to conveniently route the signals and avoid mechanical interference between the mini-flange pins and screws with the waveguide circuit.

A 3D drawing of the mechanical blocks of the new OMT prototype is shown in Fig. 24. The external dimensions of the OMT are the same as in the first prototype.

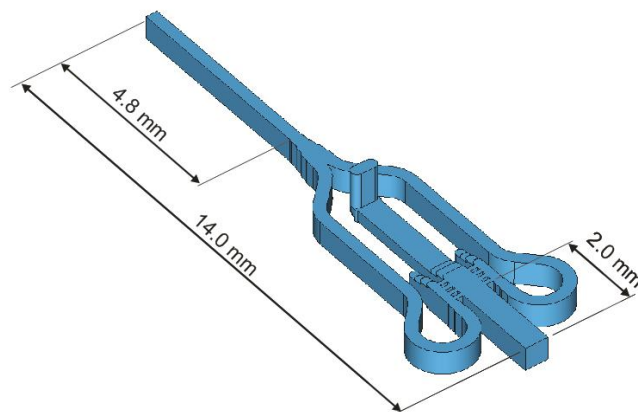


Fig. 23. Internal view of the new OMT design (full view) with short square waveguide input (2.0 mm long) and output (4.8 mm.) Custom-made mini-flanges are adopted at all ports in order to reduce the length of the waveguide sections (see Fig. 24.)

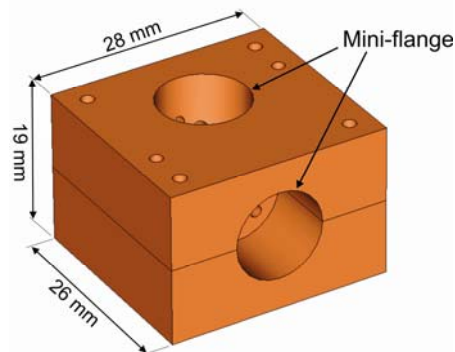


Fig. 24. Mechanical design of the second OMT prototype employing mini-flanges at all ports. The external dimensions are 19×26×28 mm³.

The results of electromagnetic simulation of the second OMT prototype are shown in Figs. 25-27. Three different cases were analysed with OMT block halves laterally misaligned of: $\delta=0 \mu\text{m}$ (perfectly aligned OMT), $\delta=2 \mu\text{m}$, $\delta=5 \mu\text{m}$.

The simulated input reflections (Fig. 25) depend weakly on δ and are below -17 dB across the 385-500 GHz band.

Fig. 26 shows the simulated transmission of the device, which is about -0.25 dB for Pol 1 and about -0.65 dB for Pol 2. In particular, the transmission is greater than in the first OMT prototype and depends much more weakly on δ (see Fig. 5 and Fig. 19 for comparisons.) This is a considerable advantage of this new design.

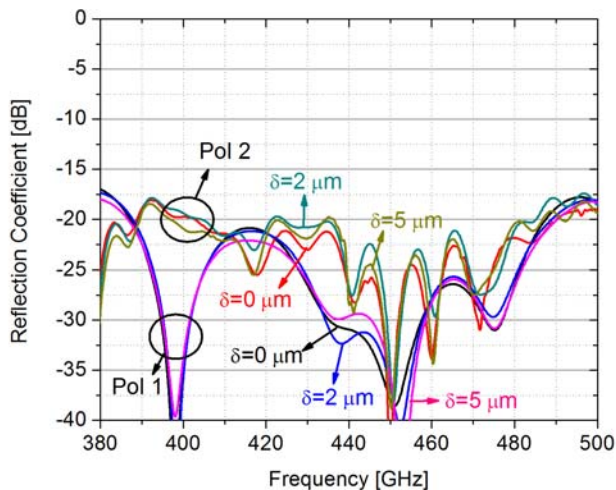


Fig. 25. Simulated input reflection coefficient of the second OMT prototype of Fig. 23 with lateral misalignments $\delta=0, 2,$ and $5 \mu\text{m}$.

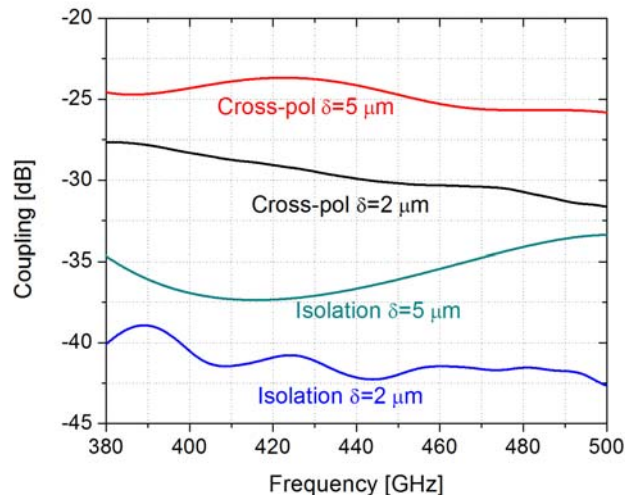


Fig. 27. Simulated cross-polarization and isolation of the second OMT prototype of Fig. 23 with lateral misalignments $\delta=2$ and $5 \mu\text{m}$.

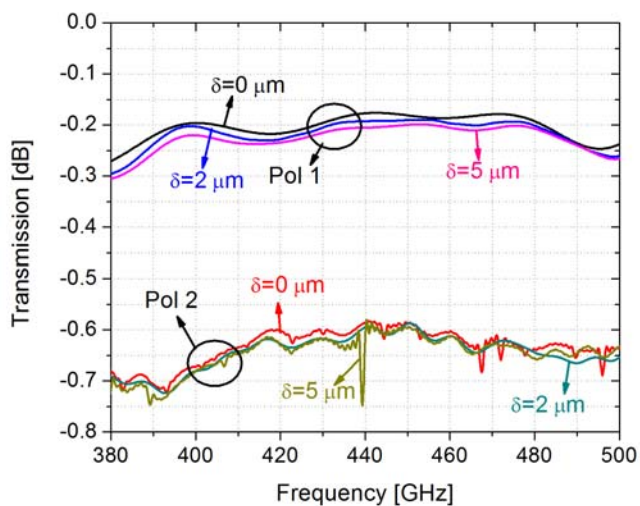


Fig. 26. Simulated transmission of the second OMT prototype of Fig. 23 with lateral misalignments $\delta=0, 2,$ and $5 \mu\text{m}$. We assumed the waveguide conductor to have perfectly smoothed walls with conductivities $\sigma=4.26 \cdot 10^7 \Omega^{-1}\text{m}^{-1}$ (300 K.)

The simulated cross-polarization and isolation of the OMT are shown in Fig. 27. With a misalignment $\delta=5 \mu\text{m}$ the cross-polarization is approximately -25 dB, much lower than in the first OMT prototype, where a value of approximately -10 dB was predicted (see Fig. 21.) The cross-pol would reduce to ≈ -30 dB with $\delta=2 \mu\text{m}$. The simulated isolation is of order -35 dB and -42 dB for, respectively $\delta=2 \mu\text{m}$ and $5 \mu\text{m}$.

Ideally, if we could reduce the length of the square waveguide input of the OMT in Fig. 23 from 2 mm to zero (which would be impossible to fabricate) the predicted cross-polarization level with a lateral misalignment $\delta=5 \mu\text{m}$ between block halves would reduce to approximately -30 dB.

VII. CONCLUSIONS

We have presented the design, construction, and test of a 385-500 GHz waveguide OMT based on a symmetric reverse-coupling structure. The OMT was fabricated in split-block technique using a numerically controlled milling machine.

The OMT was tested at JPL using a sub-mm VNA. The measured room temperature insertion loss was approximately 2 dB, the reflection was less than -10 dB, the isolation was less than -25 dB, and the cross-polarization level was less than -10 dB for both polarization channels.

Electromagnetic simulation of the OMT, obtained with a commercial software, predicted considerably better performance.

We investigated the effects of misalignments between OMT block halves using simulation and found that even a small alignment error of $5 \mu\text{m}$ can explain most of the measured effects.

Starting from the first prototype, we designed a second OMT that has shorter input and output waveguides and is much more tolerant to misalignment errors. The second OMT prototype is expected to have considerably improved performance over the first prototype. The new OMT is being fabricated and will be tested soon.

REFERENCES

- [1] G. Chattopadhyay, B. Philhour, J. E. Carlstrom, S. Church, A. Lange, and J. Zmuidzinas, "A 96-GHz Ortho-Mode Transducer for Polatron", *IEEE Microwave and Guided Wave Letters*, vol. 8, no. 12, pp. 421-423, Dec. 1998.
- [2] A. Dunning, S. Srikanth, and A.R. Kerr, "A Simple Orthomode Transducer for Centimeter to Submillimeter Wavelengths", *Proceedings of the 20th International Symposium on Space Terahertz Technology*, Charlottesville, Apr. 2009, pp. 191-194.
- [3] A. M. Boïfot, E. Lier, T. Schaug-Pettersen, "Simple and Broadband Orthomode Transducer," *Proceedings IEE*, 1990, vol. 137, n. 6, pp. 396-400.

- [4] E. J. Wollack and W. Grammer, "Symmetric Waveguide Orthomode Junctions," *Proceedings of the 14th International Symposium on Space Terahertz Technology*, Tucson, Arizona, Apr. 2003, pp.169-176.
- [5] G. Narayanan and N. Erickson, "Full-Waveguide Band Orthomode Transducer for the 3 mm and 1mm Bands," *Proceedings of the 14th International Symposium on Space Terahertz Technology*, Tucson, Arizona, Apr. 2003, pp. 508-512.
- [6] A. Navarrini and M. Carter, "Design of a Dual Polarization SIS Sideband Separating Receiver Based on Waveguide OMT for the 275-370 GHz Frequency Band," *Proceedings of the 14th International Symposium on Space Terahertz Technology*, Tucson, Arizona, Apr. 2003, pp. 159-168.
- [7] A. Navarrini and R. L. Plambeck, "A Turnstile Junction Waveguide Orthomode Transducer," *IEEE Trans. Microwave Theory Tech.*, vol. 54, n. 1, pp. 272-277, Jan. 2006.
- [8] A. Navarrini A. Bolatto, R. L. Plambeck, "Test of 1 mm Band Turnstile Junction Waveguide Orthomode Transducer", *Proceedings of the 17th International Symposium on Space Terahertz Technology*, Paris, France, May 10-12, 2006, pp. 99-102.
- [9] G. Pisano, L. Pietranera, K. Isaak, L. Piccirillo, B. Johnson, B. Maffei, S. Melhuish, "A Broadband WR10 Turnstile Junction Orthomode Transducer," *IEEE Microwave and Wireless Components Letters*, vol. 17, n. 4, pp. 286-288, April 2007.
- [10] G. G. Moorey, P. Axtens, M. Bowen, A. Dunning, R. Gough, G.R. Graves, H. Kanoniuk, "A 77-117 GHz cryogenically cooled receiver for radioastronomy," *Workshop in Applications of Radio Science (WARS2006)*, Leura, NSW, 15-17 Feb. 2006.
- [11] S. Asayama, "Double-Ridged Orthomode Transducer for ALMA Band 4 receiver," *Technical Memo of National Astronomical Observatory of Japan NINS*, 27 Feb. 2007.
- [12] O. A. Peverini, R. Tascone, G. Virone, A. Olivieri, R. Orta, "Orthomode Transducer for Millimeter-Wave Correlation Receivers," *IEEE Trans. Microwave Theory Tech.*, vol. 54, n. 5, May 2006, pp. 2042-2049.
- [13] A. Navarrini, R. Nesti, "Symmetric reverse-coupling waveguide orthomode transducer for the 3 mm band," *IEEE Trans. Micr. Theory and Tech.*, vol. 57, n. 1, Jan 2009, pp. 80-88.
- [14] M. Kamikura, M. Naruse, S. Asayama, N. Satou, W. Shan, and Y. Sekimoto "Development of a 385-500 GHz Orthomode Transducer (OMT)," *Proceedings of the 19th International Symposium on Space Terahertz Technology*, Groningen, The Netherlands, Apr. 2008, pp 557-562.
- [15] C. Groppi, C. Y. Drouet d-Aubigny, A. W. Lichtenberger, C. M. Lyons, C. K. Walker, "Broadband Finline Ortho-Mode Transducer for the 750-1150 GHz Band," *Proceedings of the 16th International Symposium on Space Terahertz Technology*, Chalmers, May 2005, pp. 513-518.
- [16] A. R. Kerr, "Elements for E-plane Split-Blocks Waveguide Circuits," National Radio Astronomy Observatory, *ALMA Memo* No. 381, Jul. 2001.
- [17] A. R. Kerr, "Effects of misalignment of square waveguide joints," National Radio Astronomy Observatory, *EDTN 211*, 12 March 2009. Available at: <http://www.gb.nrao.edu/electronics/edtn/edtn211.pdf>